



Removal of naproxen and diclofenac using magnetic nanoparticles/nanocomposites

Muradiye Şahin¹ · Yasin Arslan² · Fatma Tomul³

Received: 21 August 2022 / Accepted: 24 October 2022 / Published online: 1 November 2022
© The Author(s), under exclusive licence to Springer Nature B.V. 2022

Abstract

Magnetic iron oxide and iron/copper nanoparticles were synthesized using *Lathyrus brachypterus* extract, and then magnetic Fe₃O₄-CS, Fe₃O₄-AT, Fe/Cu-CS and Fe/Cu-AT nanocomposite beads were synthesized using chitosan and alginate natural polymers. They were used for both adsorption and heterogeneous catalysts for the catalytic wet peroxidation (CWPO) of naproxen (NPX), diclofenac (DCF) and NPX + DCF drugs which are important micro-organic pollutants, separately and together (NPX + DCF) from aqueous media. In adsorption studies, the drugs were adsorbed very quickly in the first minutes and then, desorbed in between 8 and 10 min. In competitive adsorption, the adsorbents showed selective properties for DCF and NPX. In CWPO technique, drug removal was achieved in 9 min with a conversion capacity of 92% for DCF with Fe/Cu-CS and 84% for NPX with Fe/Cu-AT optimum experimental conditions, such as pH 5, 30% of H₂O₂, 100 mg catalyst and 298 K. Based on reusability of the catalysts, it was seen that there was a slight decrease in the removal efficiencies in the third cycle and the stable and active structure of the catalyst was preserved to the desired extent. Furthermore, the oxidation reaction was in good agreement with the pseudo-first-order kinetic model.

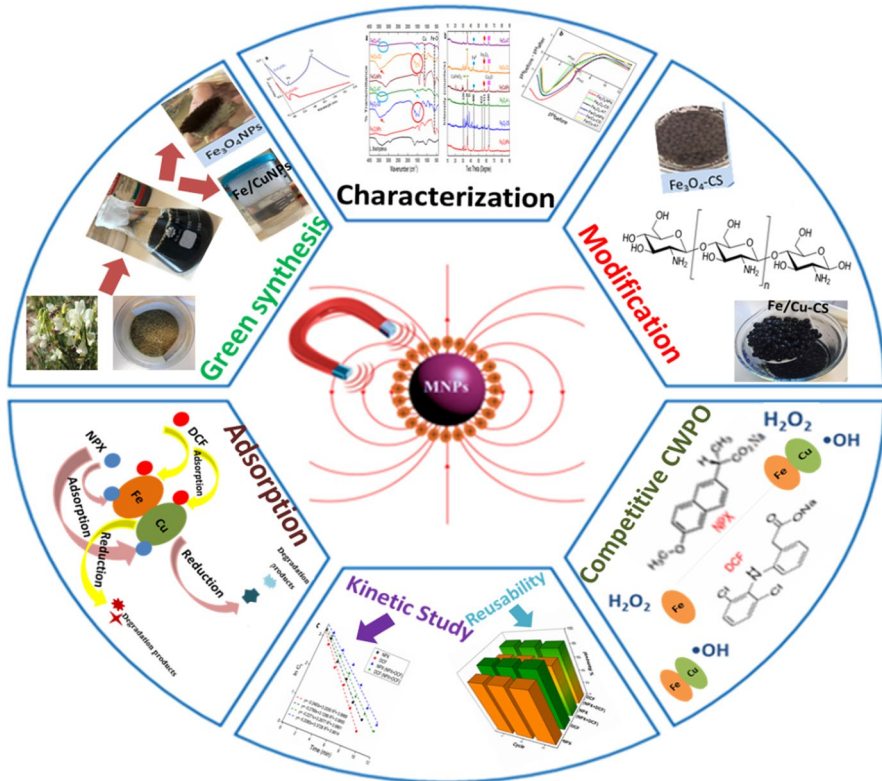
✉ Yasin Arslan
yasinarslan@mehmetakif.edu.tr

¹ Campus, Kırşehir Ahi Evran University, 40100 Kırşehir, Turkey

² Department of Nanoscience and Nanotechnology, Faculty of Arts and Science, Burdur Mehmet Akif Ersoy University, 15030 Burdur, Turkey

³ Department of Chemistry, Faculty of Arts and Science, Burdur Mehmet Akif Ersoy University, 15030 Burdur, Turkey

Graphical abstract



Keywords Adsorption · Oxidation · Magnetic nanoparticles/nanocomposites · Drug removal

Introduction

The rapid increase in the world population and limited resources have made the growth of industrialization inevitable [1]. Accordingly, the rate of getting sick in humans is constantly increasing due to many reasons, such as living areas becoming industrial areas, inadequacy of healthy foods and difficulties in accessing these foods, fast and stressful life [2]. On the other hand, in addition to the usual processes, extraordinary pandemic situations (such as the COVID-19 epidemic that has been going on for more than 2 years) cause a sudden and very significant increase in the disease process. Due to the increase in disease rates, increasing global drug production and high consumption of drugs cause the pollution of natural water resources, drinking water and wastewater by pharmaceutical components, making this an important environmental problem [1, 2]. Among the pharmaceutical

components, “nonsteroidal anti-inflammatory” drugs, which have analgesic and antipyretic effects, are the most widely used group of drugs with the highest environmental pollution risk [3–5]. Naproxen sodium (NPX) is one of the most consumed active pharmaceutical ingredients in this group [6, 7]. Studies conducted on living things have determined that NPX adversely affects especially aquatic organisms that even low doses can be fatal for embryos and larvae [8, 9], and there is even a risk of damaging the genetic structures of living things [10]. Diclofenac sodium (DCF), which prevents the inflammatory reaction, has painkiller (analgesic) and antipyretic (antipyretic) effects; it is a nonsteroidal anti-inflammatory drug. DCF is used in the treatment of headache, chronic muscle pain and arthritic pain [11–13]. Since DCF is the chemical with the highest acute effect among the chemicals with an anti-inflammatory nature, it is of great importance in terms of environmental risk [14]. Studies have reported changes in liver, kidney and gill cells, deterioration in kidney tissue and changes in gill structures in fish [15]. Delays and failures in the hatching process were observed in fish exposed to 0.01–10 mg/L DCF concentration [16]. Therefore, NPX and DCF are considered to be effective environmental pollutants in terms of their potential to adversely affect living organisms and pose a threat to living things in the natural environment. For these reasons, the removal of NPX and DCF from aqueous media is very important and remarkable.

Many techniques, such as chlorination [17], coagulation/sedimentation [18, 19], ozonation [20–22], oxidation [23–26], biofiltration [27–29], adsorption [3, 30–34], have been used for drug removal from aqueous media. Among these methods, adsorption and catalytic wet peroxidation (CWPO) have an important place with the advantages of easy application, economic and effective removal potential [35–37]. Hydrogen peroxide as an oxidation agent during the degradation of organic substances by CWPO method is an environmentally friendly oxidant that does not cause harmful by-product formation, and hydroxyl radicals are formed by the decomposition of hydrogen peroxide with the effect of catalyst and heat.

In this study, magnetic iron oxide (Fe_3O_4 NPs) and iron/copper (Fe/CuNPs) nanoparticles were synthesized using an endemic plant species, *Lathyrus brachypterus* extract, with a fast, economical, harmless to human health, and environmentally friendly green synthesis method. The synthesized magnetic nanoparticles were separately modified with chitosan and alginate natural polymers. The magnetic nanoparticles/nanocomposites were characterized by FTIR, TEM, XRD, SEM–EDX and UV–VIS techniques. To the best of our knowledge, this is the first study because magnetic nanoparticles/nanocomposites were synthesized using endemic *Lathyrus brachypterus* plant extract, and they were used for both adsorbent and catalyst to remove separately and together of both DCF and NPX from aqueous media. Magnetic nanoparticles were preferred because of their high catalyst loading capacity, high dispersion property, high stability, recyclability and high surface area properties. In addition, the recovery of the catalyst from the liquid-phase reaction medium by magnetic separation is easier than filtration and centrifugation, and it is very convenient in terms of reducing the time. Various experimental parameters such as pH_{pzc}, temperature and H_2O_2 amount were optimized to investigate the adsorption and oxidation processes of NPX, DCF and NPX+DCF in aqueous solution with magnetic nanoparticles/nanocomposites. The synthesized

nanoparticles and nanocomposites could be easily dispersed in the environment and collected quickly with the help of a magnet without losing efficiency for removal of drugs.

Materials and methods

Materials and reagents

Iron (II) sulphate heptahydrate ($\text{FeSO}_4 \cdot 7\text{H}_2\text{O}$), iron (III) chloride hexahydrate ($\text{FeCl}_3 \cdot 6\text{H}_2\text{O}$) hydrogen peroxide (H_2O_2), sodium hydroxide (NaOH), diclofenac sodium ($\text{C}_{14}\text{H}_{10}\text{Cl}_2\text{NNaO}_2$) and chitosan were received from Sigma-Aldrich. Acetic acid (CH_3COOH) and sodium alginate ($\text{C}_6\text{H}_7\text{O}_6\text{Na}$) were received from Merck. Calcium chloride (CaCl_2) was received from Fluka. Naproxen sodium ($\text{C}_{14}\text{H}_{13}\text{NaO}_3$) was received from Acros Organics. Copper (II) sulphate pentahydrate ($\text{CuSO}_4 \cdot 5\text{H}_2\text{O}$) was received from Indosaw. Double-distilled water was used throughout all experimental studies (18.2 M Ω cm). All of the materials were in analytical reagent grade and utilized as received without any purification.

Characterization techniques

The chemical and morphological characterizations for the nanoparticles were realized by Shimadzu UV-1800 (UV–VIS), PerkinElmer Frontier model FT-IR, Bruker D8 Advance model X-ray diffraction (XRD) with a Cu K_α radiation source in 2θ range from 10° to 90° , TEM-120 kV transmission electron microscope (TEM) and Carl Zeiss EVO-LS 10 scanning electron microscope (SEM). Common drift method [30] was used to determine the pH (pHpzc) of nanoparticles and nanocomposites at the zero charge point. For this, 50 mL of 0.01 M NaCl solution was placed in a closed flask. The pH value was adjusted to a value between 2.0 and 12.0 by adding 0.1 M HCl and/or 0.1 M NaOH solutions. Then, 0.05 g of each nanoparticles/nanocomposites was added, and the final pH was measured using the pH meter (Thermo Scientific, Orion 3 Star) after 24 h under shaking at room temperature. The intersection point of initial pH and final pH values was determined to be pHpzc.

Synthesis of Fe_3O_4 NPs and Fe/CuNPs

One gram of ground *Lathyrus brachypterus* plant was weighed and added to 50 mL of distilled water. Then, the mixture was stirred continuously at 25°C for 5 h and filtrated using a Whatman No 1 filter paper (90 mm, 82 g/m² and pore size: 15–19 μm) to obtain plant extract. For the synthesis of Fe_3O_4 NPs, 100 mL solution including 0.56 g $\text{FeSO}_4 \cdot 7\text{H}_2\text{O}$ and 0.81 g $\text{FeCl}_3 \cdot 6\text{H}_2\text{O}$ was prepared and 10 mL of the plant extract was added to the prepared solution. For the synthesis of Fe/CuNPs, 100 mL solution including 1.38 g $\text{FeSO}_4 \cdot 7\text{H}_2\text{O}$ and 0.69 g $\text{CuSO}_4 \cdot 5\text{H}_2\text{O}$ was

prepared and 10 mL of the plant extract was added to the prepared solution. Then, they were mixed at room temperature for 30 min at 500 rpm on a magnetic stirrer and left to settle. The resulting Fe_3O_4 and Fe/Cu nanoparticles were separated from the filtrate with a magnet and washed three times with distilled water and dried in an oven.

Synthesis of Fe_3O_4 -CS and Fe/Cu-CS

0.50 g of chitosan was mixed with 50 mL of 1% acetic acid until a homogeneous mixture was obtained. Then, 0.40 g of the synthesized magnetic Fe_3O_4 NPs was added to this mixture and dropped into 100 mL of 1 M NaOH solution with a dropper to form Fe_3O_4 -CS beads. The formed beads were kept in NaOH for 12 h, washed with distilled water. At the end of the period, half of them were kept in distilled water at 4 °C, and the other half was dried in an oven at 50 °C to compare their adsorption and oxidation effects separately. The same process was performed by replacing Fe_3O_4 NPs with Fe/CuNPs for the synthesis of Fe/Cu-CS.

Synthesis of Fe_3O_4 -AT and Fe/Cu-AT

0.60 g of sodium alginate was mixed with 50 mL of distilled water until a homogeneous solution was formed. 0.50 g Fe_3O_4 NPs was added to the prepared mixture and sonicated for 30 min. Then, Fe_3O_4 -AT beads were formed by dropping the obtained homogeneous solution into 2% of CaCl_2 solution. The obtained beads were washed with distilled water. At the end of the period, half of them were kept in distilled water at 4 °C, and the other half was dried in an oven at 50 °C to compare their adsorption and oxidation effects separately. The same process was performed by replacing Fe_3O_4 NPs with Fe/CuNPs for the synthesis of Fe/Cu-AT.

Adsorption experiments

Adsorption of NPX, DCF and NPX+DCF on magnetic nanoparticles/nanocomposites was carried out using the batch adsorption method. For this, 25 mg adsorbents was separately mixed with 30 mL of 25 mg/L drug solutions in 50 mL falcon tubes at pH=5 and 298 K. Then, all tubes were mixed at 250 rpm for 10 min, and the drug concentrations remaining unadsorbed in the solution were determined by measuring the absorbances for NPX and DCF at 272 nm and 254 nm, respectively, with a UV-VIS spectrophotometer [38, 39].

Catalytic wet peroxidation of NPX, DCF and NPX + DCF

To investigate the catalytic activities of nanoparticles/nanocomposites for NPX, DCF and NPX + DCF, there different solutions containing 100 mL of 25 mg/L NPX, 100 mL of 25 mg/L DCF and 100 mL of 25 mg/L NPX and 25 mg/L DCF mixture were separately prepared. The catalytic process was started by adding both 3 mL of freshly prepared 30% H_2O_2 and 0.1 g magnetic nanoparticles/nanocomposites

catalyst to all these solutions, and they were mixed with a magnetic stirrer at 250 rpm. Then, 3 mL of sample was separately taken at regular intervals, separated from the catalyst by magnet, mixed with a 1 mL of distilled water and then UV–VIS measurements were taken. The oxidation experiments were carried out at pH=5 at room temperature. Catalytic activities of Fe₃O₄-CS, Fe₃O₄-AT, Fe/Cu-CS and Fe/Cu-AT beads stored both in pure water at 4 °C and dried in an oven at 50 °C were also compared, and it was seen that the ones stored in pure water at 4 °C gave better catalytic activity. Therefore, those stored in pure water at 4 °C were used in all further studies. To determine catalytic activities of nanoparticles/nanocomposites for NPX, DCF and NPX + DCF, some experimental conditions, such as catalyst amount (50 mg, 100 mg, 150 mg and 200 mg), pH (2, 4, 5 and 6), temperature (298 K, 313 K and 328 K) and H₂O₂ concentration (30%, 40% and 50%), were optimized and found to be 100 mg catalyst, pH 5, 298 K and 30% of H₂O₂, respectively. Furthermore, reusability of catalysts and reaction kinetics were investigated in detail.

Results and discussion

Characterization

The peaks seen in UV–VIS (Fig. 1a) is the characteristic peaks of Fe₃O₄NPs and Fe/CuNPs, and it was confirmed that the nanoparticles were successfully synthesized [40, 41]. The pH_{pzc} values of Fe₃O₄NPs, Fe₃O₄-CS, Fe₃O₄-AT, Fe/CuNPs, Fe/Cu-CS and Fe/Cu-AT were found to be 6.47; 5.18; 5.65; 6.32; 5.54 and 5.87, respectively (Fig. 1b). The studies were carried out at pH=5, which is below the pzc

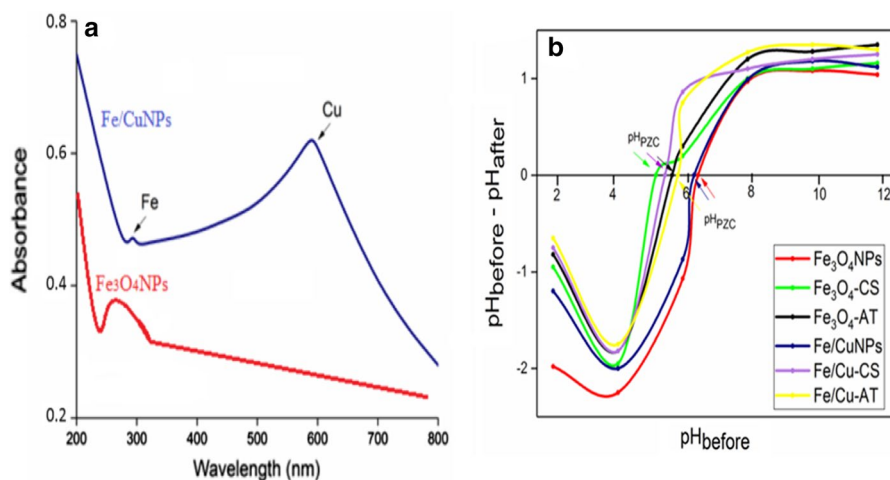


Fig. 1 **a** UV–VIS spectra of Fe/CuNPs and Fe₃O₄NPs (conditions: plant extract volume 10 mL, 1.38 g FeSO₄·7H₂O, 0.18 g CuSO₄·5H₂O, 25 °C and 0.56 g FeSO₄·7H₂O, 0.81 g FeCl₃·6H₂O) and **b** pH_{pzc} of the adsorbents (conditions: 50 mg each nanoparticles/nanocomposites, 50 mL 0.01 M NaCl, 25 °C and 24 h)

value for all adsorbents. If the pH is below the pH_{pzc} value, the surface charge of the adsorbent becomes positive, so anions can be adsorbed [42]. Since the pK_a values of DCF and NPX were around 4.1 [42] and 4.2 [30], respectively, and both pK_a values for drugs are lower than the solution pH, both drugs are in anionic form and so there is electrostatic attraction with the adsorbent [42].

FTIR results of Fe/CuNPs, Fe/Cu-CS, Fe/Cu-AT, Fe_3O_4 NPs, Fe_3O_4 -CS, Fe_3O_4 -AT and *L. Brachypterus* extract are given comparatively in Fig. 2a. The characteristic peak at 555 cm^{-1} seen in all nanoparticles FT-IR spectra is due to the stretching vibration of the Fe–O bond [43, 44], and the characteristic peak at 1008 cm^{-1} is due to the presence of Cu [45]. The peak seen at 3465 cm^{-1} in the FT-IR spectrum of both Fe/Cu-CS and Fe_3O_4 -CS belongs to the –NH or –OH asymmetric vibration of chitosan. The width of this peak is due to the presence of hydrogen bonding in the nanocomposite. A H bond is formed by attaching the –NH or –OH group of pure chitosan to the –OH group of acetic acid [46]. Apart from these, the stretching vibration of C=O at 1732 cm^{-1} , the C–O–C bonds of the polysaccharide skeleton at 1028 cm^{-1} and the characteristic peaks of β -1,4-glycosidic bond at 1153 and 895 cm^{-1} show that chitosan is present in the structure [47]. In the FT-IR spectrum of both Fe/Cu-AT and Fe_3O_4 -AT, O–H stretches at 3313 cm^{-1} , asymmetric and symmetrical stresses due to –COO at 1595 and 1417 cm^{-1} , –O–C–O– stretches of ether groups and –C–O– stretches of alcohol groups at 1100 – 1300 cm^{-1} indicate that there is alginate in the structure [48–50].

The X-ray diffraction patterns of Fe/CuNPs, Fe/Cu-CS, Fe/Cu-AT, Fe_3O_4 NPs, Fe_3O_4 -CS and Fe_3O_4 -AT magnetic nanoparticles are shown in Fig. 2b. In the XRD pattern of Fe/CuNPs, four peaks corresponding to $2\theta=37.4$, 44.6 , 57.8 and 61.4 angle values belong to CuFeO_2 , zero-valent iron (Fe^0), Fe_2O_3 and Cu_2O , respectively [51–54]. The particle size of Fe/CuNPs was calculated as 18.05 nm from the Debye–Scherrer equation using the peak intensity observed at $2\theta=37.4$

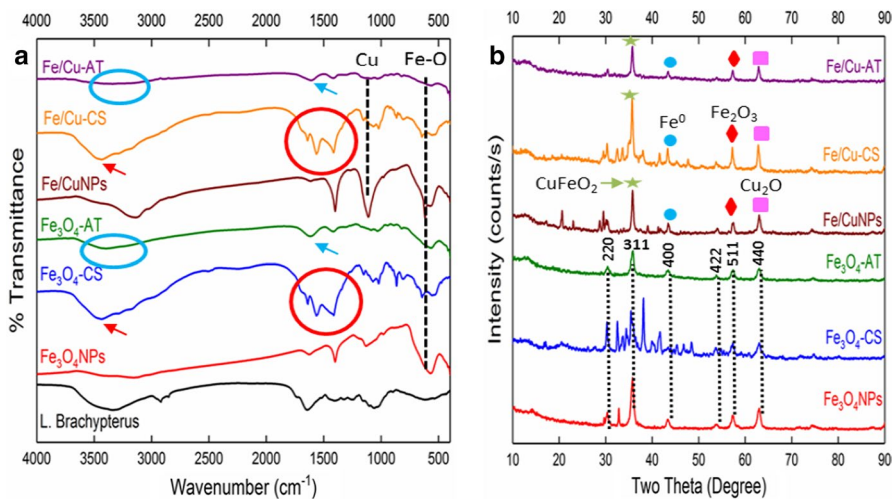


Fig. 2 a FTIR spectrum and b XRD models of nanoparticles/nanocomposites

in the diffraction pattern of these nanoparticles. In the XRD pattern of $\text{Fe}_3\text{O}_4\text{NPs}$, six peaks belonging to the crystal structures 220, 311, 400, 422, 511 and 440 were observed, corresponding to the angle values of $2\theta=30.18, 35.47, 43.30, 53.42, 57.18$ and 62.70 (JCPDS 65-3107). The particle size of $\text{Fe}_3\text{O}_4\text{NPs}$ was calculated as 11.02 nm from the Debye–Scherrer equation using the peak intensity observed at $2\theta=35.47$ in the diffraction pattern of these nanoparticles. The four peaks detected in the XRD pattern of Fe/CuNPs were also detected in the diffraction pattern of both Fe/Cu-CS and Fe/Cu-AT nanocomposites, and six peaks detected in the XRD pattern of $\text{Fe}_3\text{O}_4\text{NPs}$ were also detected in the diffraction pattern of both $\text{Fe}_3\text{O}_4\text{-CS}$ and $\text{Fe}_3\text{O}_4\text{-AT}$ nanocomposites. This result showed that the coating of both Fe/CuNPs and $\text{Fe}_3\text{O}_4\text{NPs}$ with chitosan and alginate did not change the crystal structure.

The shape and size of the Fe/CuNPs were also determined by TEM and SEM analysis (Fig. 3a–d). The SEM images show individualistic Fe/CuNPs besides a series of aggregates (Fig. 3b). The map data of elemental mapping confirmed the presence of Fe and Cu and are consistent with the SEM images (Fig. 3b, c). In addition, as seen from the EDX analysis results (Fig. 3d), it was confirmed that the bimetallic nanoparticle was synthesized with a ratio including both 58.06% Fe and 35.76% Cu in the structure. TEM images (Fig. 3a) obviously show that the nanoparticles are nearly spherical in shape. Figure 3a also indicates the size

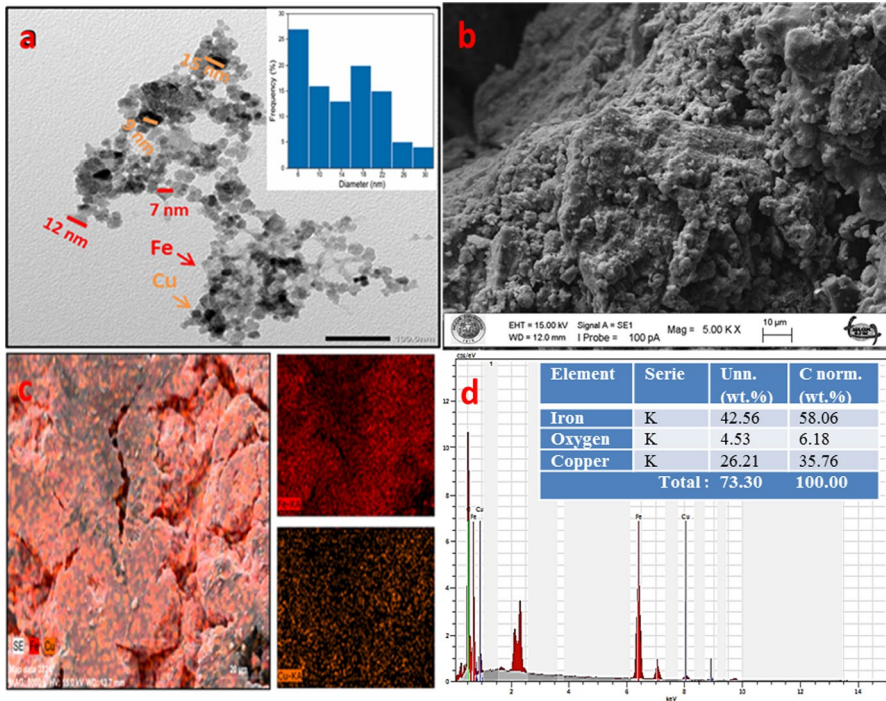


Fig. 3 a TEM images and histograms of Fe/CuNPs b SEM images of Fe/CuNPs c elemental mapping of Fe/CuNPs and d EDX analysis of Fe/CuNPs

distribution histogram of the particles and the mean size of the particles is found to be 18.05 ± 0.04 nm and the size of the nanoparticles varies between 6 and 30 nm and showed superparamagnetic property [55, 56]. As seen, there is a good agreement with the particle sizes calculated by the Scherrer equation in the XRD spectra shown in Fig. 2b.

The shape and size of the Fe_3O_4 NPs were also determined by TEM and SEM analysis (Fig. 4a–c). The SEM images show individualistic Fe_3O_4 NPs besides a series of aggregates. The map data of elemental mapping confirmed the presence of Fe and O and are consistent with the SEM–EDX images (Fig. 4a, c) [44, 57]. From TEM images (Fig. 4b), it is obviously seen that the nanoparticles are nearly spherical in shape. Figure 4b also indicates the size distribution histogram of the particles and the mean size of the particles is found to be 11.02 ± 0.15 nm, and the size of the nanoparticles varies between 5 and 42 nm and showed superparamagnetic property [55, 56]. As seen, there is a good agreement with the particle sizes calculated by the Scherrer equation in the XRD spectra shown in Fig. 2b.

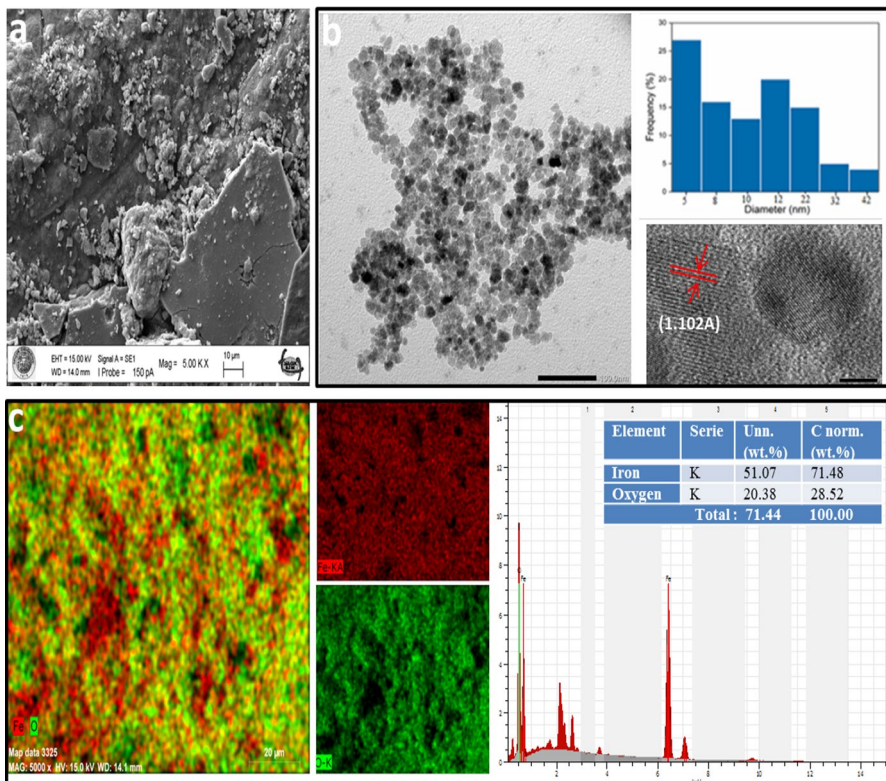


Fig. 4 a SEM images of b TEM, HR-TEM and histograms of c EDX and elemental mapping of Fe_3O_4 NPs

Adsorption capacity of nanoparticles/nanocomposites for NPX, DCF and NPX + DCF

The adsorption of 25 mg/L 30 mL of NPX, DCF and NPX+DCF by separately using 25 mg of Fe_3O_4 NPs, Fe_3O_4 -CS, Fe_3O_4 -AT, Fe/CuNPs, Fe/Cu-CS and Fe/Cu-AT magnetic nanoparticles at room temperature was investigated, and the results are given in Fig. 5a–d. As can be seen from Fig. 5, adsorption capacity of Fe/CuNPs bimetallic nanoparticle adsorbent for NPX, DCF and NPX + DCF is higher than that of Fe_3O_4 NPs. It was also observed that adsorption capacity of nanocomposites for NPX, DCF and NPX+DCF is higher than that of nanoparticles. As the nanocomposites have larger surface area, more porosity and more functional groups with respect to nanoparticles, the adsorption capacity of them is higher than that of nanoparticles [48, 50]. However, during the adsorption studies, it was observed that the fact drugs that adsorbed rapidly in the first minutes were desorbed again in the first 10 min reveals that the interaction between the adsorbate and the adsorbent is the type of physical adsorption explained by the van der Waals force [58–62], and

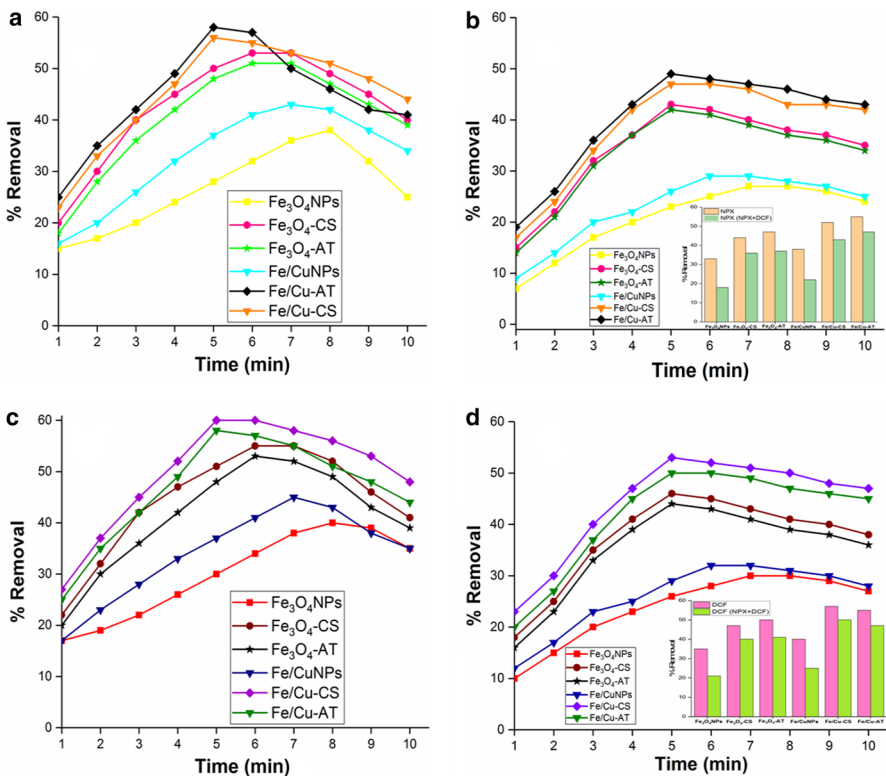


Fig. 5 Comparative **a** NPX **b** NPX (NPX+DCF) **c** DCF and **d** DCF (NPX+DCF) adsorption of Fe_3O_4 NPs, Fe_3O_4 -CS, Fe_3O_4 -AT, Fe/CuNPs, Fe/Cu-CS and Fe/Cu-AT removal efficiency (initial drug concentration: 25 mg/L, adsorbent dosage: 25 mg/50 mL, $T = 298$ K, $\text{pH} = 5$)

it is seen that the adsorption can be easily reversed due to the weak intermolecular attraction force.

As seen in Fig. 5a, c, around 60% removal efficiency for both 25 mg/L NPX and 25 mg/L DCF was separately achieved within the first 5 min. On the other hand, as seen in Fig. 5b, d (competitive adsorption), the removal efficiency of 25 mg/L NPX and 25 mg/L DCF were separately reduced to around 48% and 56%, respectively, indicating an antagonistic interaction between drug components [63]. Based on results obtained from the competitive adsorption experiments, in which NPX and DCF drugs were mixed, it was revealed that all of the nanoparticles/nanocomposites acted more selectively against DCF. The binding sites of DCF based on shape, size and having more functional groups were higher than that of NPX molecule. Therefore, these higher binding sites of DCF molecules cause higher selectivity by nanocomposites [64].

Catalytic activity of nanoparticles/nanocomposites for NPX, DCF and NPX + DCF

Because of the fact that adsorption studies for the removal of NPX, DCF and NPX + DCF were not performed efficiently due to desorption, catalytic activity of nanoparticles/nanocomposites was conducted for NPX, DCF and NPX + DCF with CWPO technique. For this, 25 mg/L of 100 mL NPX, DCF and NPX + DCF with CWPO at pH = 5 in the presence of 30% H₂O₂ as oxidation agent at room temperature were separately mixed with 100 mg of Fe₃O₄NPs, Fe₃O₄-CS, Fe₃O₄-AT, Fe/CuNPs, Fe/Cu-CS and Fe/Cu-AT magnetic nanoparticles/nanocomposites used as catalysts and the results are given in Fig. 6a–d.

Fe/Cu-CS with 92% in DCF removal and Fe/Cu-AT with 84% in NPX removal provided the highest removal. In the competitive CWPO experiment, it was observed that Fe/Cu-CS, which gave the best results in the removal of NPX + DCF drug mixture, started to remove DCF at the first and the DCF removal rate in the mixture was higher than that of NPX (Fig. 6c, d). In addition, it was observed that the individual removal efficiency of NPX and DCF was higher than the binary competitive oxidation. In general, the hydrophobic interactions played an important role in the CWPO process. NPX is a monocarboxylic acid consisting of a methoxynaphthalene, and DCF is a monocarboxylic acid consisting of the amino group and phenylacetic (2,6-dichlorophenyl). NPX (pKa = 4.2) molecule is more stable than that of DCF (pKa = 4.1), so DCF removal was observed higher in competitive oxidation.

In principle, it can be said that the decompositions of drugs by oxidation are based on the principle of producing OH[•] radicals. H₂O₂ adsorbed by the metal nanoparticle takes electrons from the metal nanoparticle and forms OH[•] radicals as a result of OH⁻ ion oxidation. These radicals adsorbed by the nanoparticle react with the drug on the surface and cause the drugs to decompose. In other words, the OH[•] radical oxidizes the drug and converts it to CO₂ and H₂O. The rate of catalytic oxidation depends on both adsorptions of H₂O₂ on the nanoparticle surface and electron transfers from the nanoparticle. It can be said that nanoparticles effectively weaken the O–O bond, providing an advantage for H₂O₂ adsorption and increasing

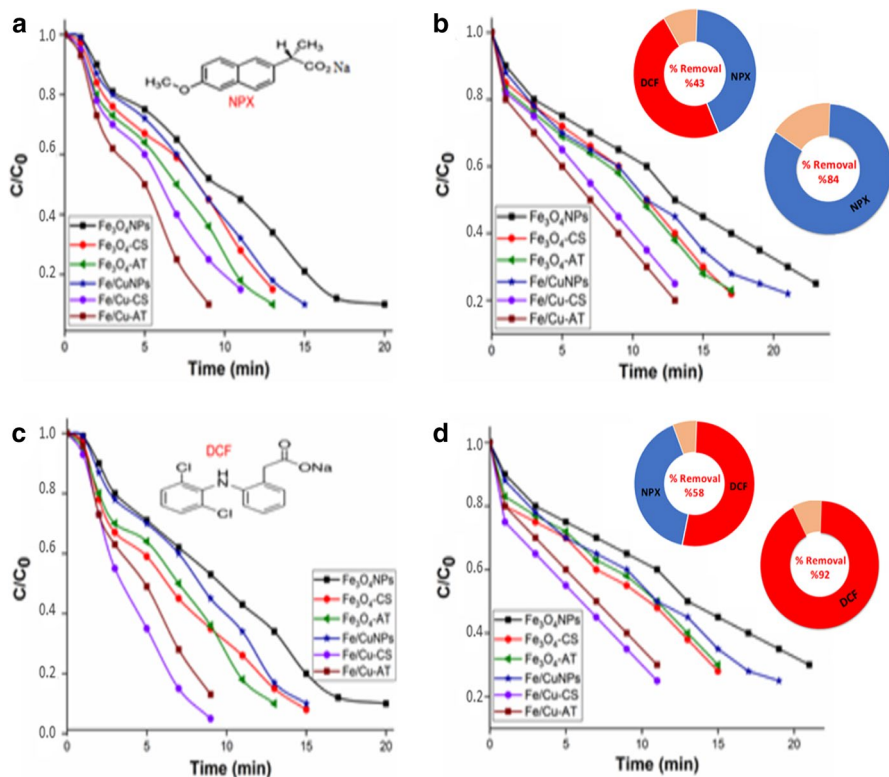


Fig. 6 Comparison of the catalytic activity Fe_3O_4 NPs, Fe_3O_4 -CS, Fe_3O_4 -AT, Fe/CuNPs, Fe/Cu-CS and Fe/Cu-AT **a** NPX **b** NPX (NPX + DCF) **c** DCF and **d** DCF (NPX + DCF) in the CWPO (initial drug concentration: 25 mg/L, catalyst dosage = 100 mg, pH = 5, $T = 298$ K)

the electron transport rate. In the literature, it has been explained that the possible oxidation reaction mechanism occurs in the presence of hydroxyl (HO^\cdot) and hydroperoxyl (HOO^\cdot) radicals formed from H_2O_2 [35].

Optimization studies were carried out with Fe/Cu-CS and Fe/Cu-AT, which provide the highest DCF and NPX removal in the shortest time, and oxidation reaction kinetics were investigated. When the experiments were performed at pH = 2, 4, 5 and 6, respectively, the best result was obtained at pH = 4, and the drug removal efficiency decreases with increasing pH (Fig. 7a). However, considering the minimum corrosion and the drug removal efficiency at pH = 5 being close to that of pH = 4, the optimum pH value was chosen as 5, and further studies were carried out at this pH. In CWPO experiments performed at 25, 40 and 55 °C, drug removal efficiency was best achieved at 25 °C (Fig. 7a). From the results obtained, the reaction is considered to be exothermic. In order to understand the effect of H_2O_2 concentration on drug removal 30, 40 and 50% (v/v) of H_2O_2 solutions were separately used. It was determined that with the increase in hydrogen peroxide concentration from 30 to 40, the decomposition

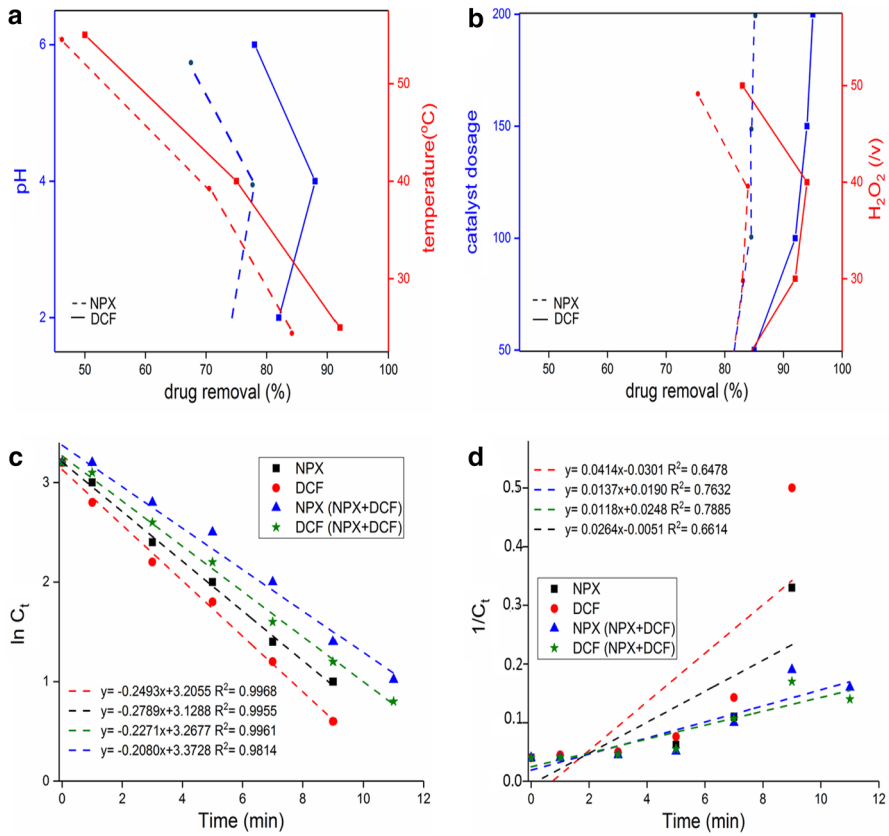
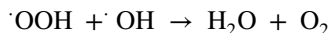
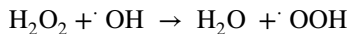


Fig. 7 Effect of **a** pH and temperature **b** catalyst dose and H₂O₂ concentration and **c** pseudo-first-order and **d** pseudo-second-order kinetic models for CWPO of NPX on Fe/Cu-AT and DCF on Fe/Cu-CS

reaction of H₂O₂ to radicals accelerated, and the drug degradation increased up to a point and then, tended to decrease as it increased from 40 to 50 (Fig. 7b). This is because at high concentrations, hydrogen peroxide prevents the formation of hydroxyl radicals, causing the reduction of these radicals. Saleh and Taufik (2019) examined the removal of methylene blue and Congo red dyes with Fe₃O₄/ZnO/graphene composite, it was found that the increase in the H₂O₂ dosage from 1 to 4 mL increases the dye removal efficiency and decreases after 4 mL dosage. Shi et al. (2018) found that the dye removal efficiency increased with the increase in the hydrogen peroxide concentration from 10 to 50 mmol/L, but the removal efficiencies decreased at the H₂O₂ concentrations of 70 mmol/L and above because the excess hydrogen peroxide reacts with the OH radicals causing the formation of OOH radicals with low-oxidation capacity. [65–67].

The reaction that takes place in the presence of excess hydrogen peroxide in the reaction medium is given below [65]:



To examine the effect of the catalyst amount, the experiments were carried out by adding 50, 100, 150 and 200 mg of magnetic Fe/Cu–CS and Fe/Cu–AT nanocomposites. As can be seen in Fig. 7b, with the increase in the amount of catalyst, the drug removal does not change much, but increases slightly. With the increase in the amount of catalyst, the number of active centers required for oxidation increases, which increases the drug removal efficiency [68, 69]. According to the pseudo-first-order kinetic model, $\ln C$ values against t were plotted, and the k_1 rate constant was determined from the slope. The graph drawn for the pseudo-first-order kinetic model is given in Fig. 7c. According to the pseudo-second-order kinetic model, t versus $1/C$ values were plotted, and the k_2 rate constant was determined from the slope. The graph obtained for the pseudo-second-order kinetic model is given in Fig. 7d. The rate constants and coefficients of determination (R^2) calculated for pseudo-first-order and pseudo-second-order kinetic models are given in Table 1.

When the coefficients of determination of the two kinetic models are compared, it is seen that the reaction kinetics with a higher R^2 value are compatible with the pseudo-first-order kinetic model. The activation energy (E_a) of the reactions for NPX, DCF, competitive NPX and competitive DCF is calculated from Eq. 1 and found to be 10.56, 8.83, 12.07 and 9.35 kJ/mol, respectively.

$$k = A e^{-E_a/RT} \quad (1)$$

The oxidation capacities of the nanocatalyst synthesized in this study and the different catalyst in the literature for the degradation of pollutants are given in Table 2.

In order to examine the reusability of the catalyst, the magnetic Fe/Cu–CS and Fe/Cu–AT catalysts, which were separated from the solution by magnet at the end of the experiment, were reused and this process was repeated for three cycles. When the results are examined, it is seen that there is a slight decrease in the

Table 1 Pseudo-first-order and pseudo-second-order model constants with the CWPO technique

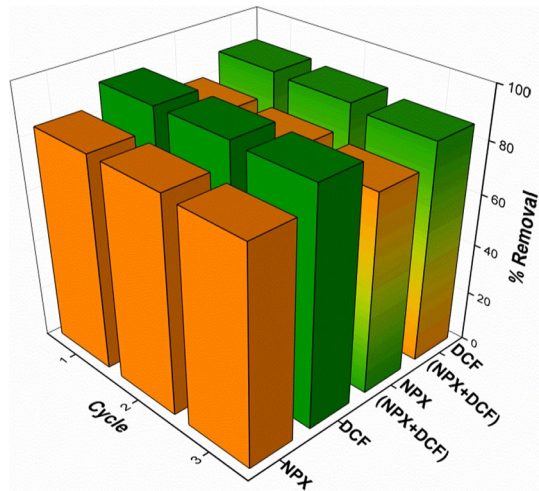
	Pseudo-first-order		Pseudo-second-order	
	k_1 (min ⁻¹)	R^2	k_2 (g L ⁻¹ min ⁻¹)	R^2
NPX*	0.2789	0.9955	0.0264	0.6614
DCF**	0.2493	0.9968	0.0414	0.6478
NPX (competitive)**	0.2080	0.9814	0.0137	0.7632
DCF (competitive)**	0.2271	0.9961	0.0118	0.7885

*Fe/Cu–AT catalyst was used

**Fe/Cu–CS catalyst was used

Table 2 A comparison of the oxidation capacity of the prepared catalyst with those announced in the literature

Pollutant	Catalyst	% Removal	Time (min.)	Reference
Phenol	Fe-AC	100	240	[70]
Orange II	Fe-AC	98	240	[71]
Orange II	Fe ₃ O ₄ NPs	70.5	180	[72]
Rhodamine B	GO-Fe ₃ O ₄	88.3	60	[73]
MB	Fe ₃ O ₄ /rGO	98.6	120	[74]
Bisphenol A	Fe ₃ O ₄ -MWCNT	90	240	[75]
Bisphenol A	FeCu-MC	93	60	[76]
Naproxen	Fe/Ti-PB	82	120	[77]
Diclofenac	Fe ₃ O ₄ -MWCNT	95	180	[78]
Naproxen	Fe/Cu-AT	84	9	Present study
Diclofenac	Fe/Cu-CS	92	9	Present study

Fig. 8 Reusability of catalysts

removal efficiencies in the third cycle, and the stable and active structure of the catalyst are preserved to the desired extent (Fig. 8).

Conclusion

Magnetic metaloxide and bimetallic nanoparticles (Fe₃O₄NPs and Fe/CuNPs) were synthesized by economical and environmentally friendly green synthesis method using the endemic plant species *Lathyrus brachypterus* extract. Characterizations of synthesized MNPs were performed. By using natural polymers, such as chitosan and alginate, nanocomposite beads (Fe₃O₄-CS, Fe₃O₄-AT, Fe/Cu-CS and Fe/Cu-AT) were synthesized. The separately or together removal of naproxen and diclofenac

which are among nonsteroidal anti-inflammatory drugs and threaten natural life from waste waters was conducted by using nanoparticles/nanocomposites used as both adsorbent and catalyst. The optimum conditions for drug removal with the highest efficiency in the shortest time were determined, and kinetic studies were carried out. All MNPs provide drug removal in CWPO studies but it was observed that Fe/Cu–CS for DCF removal and Fe/Cu–AT for NPX removal gave the best results. Furthermore, it was found that adsorption of both NPX and DCF on nanoparticle and nanocomposite beads was occurred as physical bonding.

Author contributions All authors contributed to the study conception and design. Material preparation, data collection and analysis were performed by MŞ, YA and FT. The first draft of the manuscript was written by MŞ and all authors commented on the previous versions of the manuscript. All authors read and approved the final manuscript.

Funding The authors did not receive support from any organization for the submitted work.

Declarations

Conflict of interest The authors have no competing interests to declare that are relevant to the content of this article.

References

1. H. Zhou, *Econ. Inq.* **47**, 249 (2009)
2. S. Szreter, *Brit. Med. Bull.* **69**, 75 (2004)
3. J. Lach, A. Szymonik, *J. Ecol. Eng.* **20**, 241 (2019)
4. H. Suleyman, B. Demircan, Y. Karagoz, *Pharmacol. Rep.* **59**, 247 (2007)
5. N.M. Davies, J.Y. Saleh, N.M. Skjodt, *J. Pharm. Pharm. Sci.* **3**, 137 (2000)
6. G. Boyd, S. Zhang, D. Grimm, *Water Res.* **39**, 668 (2005)
7. M. Qurie, M. Khamis, F. Malek, S. Nir, S.A. Bufo, J. Abbadi, L. Scrano, R. Karaman, *Clean: Soil Air Water* **42**, 594 (2013)
8. D. Górný, U. Guzik, K. Hupert-Kocurek, D. Wojcieszynska, *Ecotox. Environ. Safe.* **167**, 505 (2019)
9. T. Ding, K. Lin, B. Yang, M. Yang, J. Li, W. Li, J. Gan, *Bioresour. Technol.* **238**, 164 (2017)
10. M. Ahmad, M. Fatima, M. Hossain, A. Mondal, *J. Pharm. Anal.* **8**, 400 (2018)
11. B. Yilmaz, *Chromatographia* **71**, 549 (2010)
12. B. Yilmaz, A. Asci, S.S. Palabiyik, *J. Chromatogr. Sci.* **49**, 422 (2011)
13. D. Vogna, R. Marotta, A. Napolitano, R. Andreozzi, M. D'Ischia, *Water Res.* **38**, 414 (2004)
14. K. Kümmerer, *Annu. Rev. Environ. Resour.* **35**, 57 (2010)
15. J. Schwaiger, H. Ferling, U. Mallow, H. Wintermayr, R.D. Negele, *Aquat. Toxicol.* **68**, 141 (2004)
16. J. Lee, K. Ji, Y.L. Kho, P. Kim, K. Choi, *Ecotox. Environ. Safe.* **74**, 1216 (2011)
17. C. Noutsopoulos, E. Koumaki, D. Mamais, M. Nika, A. Bletsou, N. Thomaidis, *Chemosphere* **119**, 109 (2015)
18. S. Suarez, J.M. Lema, F. Omil, *Bioresour. Technol.* **100**, 2138 (2009)
19. H. Asakura, T. Matsuto, *Waste Manag.* **29**, 1852 (2009)
20. J.L. Acero, K. Stemmler, U. von Gunten, *Environ. Sci. Technol.* **34**, 591 (2000)
21. D.C. McDowell, M.M. Huber, M. Wagner, U. von Gunten, T.A. Ternes, *Environ. Sci. Technol.* **39**, 8014 (2005)
22. S.A. Snyder, E.C. Wert, D.J. Rexing, R.E. Zegers, D.D. Drury, *Ozone Sci. Eng.* **28**, 445 (2006)
23. L. Feng, E. van Hullebusch, M. Rodrigo, G. Esposito, M. Oturan, *Chem. Eng. J.* **228**, 944 (2013)
24. B. Czech, P. Oleszczuk, *Chemosphere* **149**, 272 (2016)
25. G. Coria, I. Sirés, E. Brillas, J.L. Nava, *Chem. Eng. J.* **304**, 817 (2016)

26. B. Wols, C. Hofman-Caris, *Water Res.* **46**, 2815 (2012)
27. A. Binelli, S. Magni, C. Soave, F. Marazzi, E. Zuccato, S. Castiglioni, M. Parolini, V. Mezzanotte, *Ecol. Eng.* **71**, 710 (2014)
28. M. Yong, Y. Zhang, S. Sun, W. Liu, *J. Membr. Sci.* **575**, 50 (2019)
29. B. Guieysse, Z.N. Norvill, *J. Hazard. Mater.* **267**, 142 (2014)
30. F. Tomul, Y. Arslan, B. Kabak, D. Trak, E. Kendüzler, E.C. Lima, H.N. Tran, *Sci. Total Environ.* **726**, 137828 (2020)
31. W. Sun, H. Li, H. Li, S. Li, X. Ca, *Chem. Eng. J.* **360**, 645 (2019)
32. A. Karami, R. Sabouni, M. Ghommem, *J. Mol. Liq.* **305**, 112808 (2020)
33. A.A.C. Ramírez, E.R. García, R.L. Medina, J.L.C. Larios, R.S. Parra, A.M.M. Franco, *Preprints* **14**, 2293 (2021)
34. F. Korkut, D. Saloglu, *Desalination Water Treat.* **206**, 315 (2020)
35. J. Han, H.Y. Zeng, S. Xu, C.R. Chen, X.J. Liu, *Appl. Catal. A: Gen.* **527**, 72 (2016)
36. H. Kızıldağ, *Eur. J. Sci. Technol.* **21**, 43 (2021)
37. J. Wang, Y. Zhou, Y. Shao, F. He, M. Wu, H. Ni, Y. Zheng, Y. Sun, *Res. Chem. Intermed.* **45**, 1721 (2019)
38. C. Jung, J. Oh, Y. Yoon, *Environ. Sci. Pollut. Res.* **22**, 10058 (2015)
39. M.H. Beyki, M. Mohammadirad, F. Shemirani, A.A. Saboury, *Carbohydr. Polym.* **157**, 438 (2017)
40. S. Logpriya, V. Bhuvaneshwari, D. Vaidehi, R.P. SenthilKumar, R.S.N. Malar, B.P. Sheetal, R. Amsaveni, M. Kalaiselvi, *J. Nanostructure Chem.* **8**, 301 (2018)
41. A. Chaudhry, F. Bashir, S.F. Adil, S. Saif, M.R. Shaik, M.R. Hatshan, B. Shaik, *J. King Saud Univ. Sci.* **34**, 101927 (2022)
42. M. Kragović, M. Stojmenović, J. Petrović, J. Loredo, S. Pašalić, A. Nedeljković, I. Ristović, *Proced. Manuf.* **32**, 286 (2019)
43. M. Kumari, C.U. Pittman Jr., D. Mohan, *J. Colloid Interface Sci.* **442**, 120 (2015)
44. C. Yuwei, W. Jianlong, *Chem. Eng. J.* **168**, 286 (2011)
45. M. Danish, X. Gu, S. Lu, A. Ahmad, M. Naqvi, U. Farooq, X. Zhang, X. Fu, Z. Miao, Y. Xue, *Chem. Eng. Sci.* **308**, 396 (2017)
46. S. Hussain, M. Kamran, S.A. Khan, K. Shaheen, Z. Shah, H. Suo, Q. Khan, A.B. Shah, W.U. Rehman, Y.O. Al-Ghamdi, U. Ghani, *Int. J. Biol. Macromol.* **168**, 383 (2021)
47. N. Illy, M. Robitzer, R. Auvergne, S. Caillol, G. David, B. Boutevin, *J. Polym. Sci. A: Polym. Chem.* **52**, 39 (2013)
48. A. Mohammadi, H. Daemi, M. Barikani, *Int. J. Biol. Macromol.* **69**, 447 (2014)
49. Z. Ayazi, Z.M. Khoshhesab, F.F. Azhar, Z. Mohajeri, *J. Chin. Chem. Soc.* **64**, 627 (2017)
50. L. Yang, X. Ma, N. Guo, *Carbohydr. Polym.* **90**, 853 (2012)
51. C. Gkanatsiou, N. Ntalli, U. Menkissoglu-Spiroudi, C. Dendrinou-Samara, *J. Nanotechnol. Res.* **1(2)**, 43 (2019)
52. I. Othman, M. Abu Haija, F. Banat, *J. Nanomater.* **2019**, 1 (2019)
53. H.D. Omar, *Int. Lett. Chem. Phys. Astron.* **64**, 130 (2016)
54. Y. Babae, C.N. Mulligan, Md.S. Rahaman, *Environ. Earth Sci.* **76**, 650 (2017)
55. F.P. Fato, D.-W. Li, L.-J. Zhao, K. Qiu, Y.-T. Long, *ACS Omega* **4**, 7543 (2019)
56. W. Yantasee, C.L. Warner, T. Sangvanich, R.S. Adleman, T.G. Carter, R.J. Wiacek, G.E. Fryxell, C. Timchalk, M.G. Warner, *Environ. Sci. Technol.* **41**, 5114 (2007)
57. F. Sepyani, R.D.C. Soltani, S. Jorfi, H. Godini, M. Safari, *J. Environ. Manage.* **224**, 315 (2018)
58. J. Wang, X. Guo, *Chemosphere* **258**, 127279 (2020)
59. A.H. Berger, A.S. Bhowan, *Energy Proced.* **4**, 562 (2011)
60. M.K. Mondal, *Int. J. Sustain. Dev. Plann.* **3**, 377 (2008)
61. S. Lowell, J.E. Shields, *Powder Surface Area and Porosity* (Chapman and Hall, London, 1998)
62. P.W. Atkins, *Physical Chemistry*, Oxford University Press, Oxford Melbourne Tokyo (1998)
63. V.C. Srivastava, I.D. Mall, I.M. Mishra, *Chem. Eng. J.* **117**, 79 (2006)
64. M.P. Divya, Y.S. Rajput, R. Sharma, *Anal. Lett.* **43**, 919 (2010)
65. X. Shi, A. Tian, J. You, H. Yang, Y. Wang, X. Xue, *J. Hazard. Mater.* **353**, 182 (2018)
66. R. Saleh, A. Taufik, *Sep. Purif. Technol.* **210**, 563 (2019)
67. O.P. Taran, A.N. Zagoruiko, A.B. Ayushev, S.A. Yashnik, R.V. Prihod'ko, Z.R. Ismagilov, V.V. Goncharuk, V.N. Parmon, *Res. Chem. Intermed.* **41**, 9521 (2015)
68. J.H. Park, J.J. Wang, R. Xiao, N. Tafti, R.D. Delaune, D.C. Seo, *Bioresour. Technol.* **249**, 368 (2018)
69. K.K. Rubeena, P.H.P. Reddy, A.R. Lajju, P.V. Nidheesh, *J. Environ. Manage.* **226**, 320 (2018)

70. J.A. Zazo, J.A. Casas, A.F. Mohedano, J.J. Rodríguez, *Appl. Catal. B* **65**, 261 (2006)
71. J.H. Ramirez, F.J. Maldonado-Hódar, A.F. Pérez-Cadenas, C. Moreno-Castilla, C.A. Costa, L.M. Madeira, *Appl. Catal. B* **75**, 312 (2007)
72. N.A. Zubir, C. Yacou, J. Motuzas, X. Zhang, J.C. D-Costa, *Sci. Rep.* **4**, 4594 (2014)
73. Y.H. Chang, Y.F. Yao, H. Luo, L. Cui, L.J. Zhi, *Int. J. Nanomanuf.* **10**, 132 (2014)
74. C.M. Domínguez, A. Quintanilla, J.A. Casas, J.J. Rodríguez, *Sep. Purif. Technol.* **129**, 121 (2014)
75. V. Cleveland, J.-P. Bingham, E. Kan, *Sep. Purif. Technol.* **133**, 388 (2014)
76. Y. Wang, H. Zhao, G. Zhao, *Appl. Catal. B* **164**, 396 (2015)
77. F. Tomul, Y. Arslan, E. Kendüzler, *Int. J. Adv. Sci. Eng. Technol.* **5**, 48 (2017)
78. Y. Huacalco, S. Alvarez-Torrellas, M.P. Marin, M.V. Gil, M. Larriba, V.I. Agueda, G. Ovejero, J. Garcia, *Environ. Sci. Pollut. Res.* **26**, 22372 (2019)

Publisher's Note Springer Nature remains neutral with regard to jurisdictional claims in published maps and institutional affiliations.

Springer Nature or its licensor (e.g. a society or other partner) holds exclusive rights to this article under a publishing agreement with the author(s) or other rightsholder(s); author self-archiving of the accepted manuscript version of this article is solely governed by the terms of such publishing agreement and applicable law.